Electronic Supplementary Material (ESI) for Green Chemistry.

Supporting Information (SI)

TITLE: Stimuli-Responsive/Rheoreversible Hydraulic Fracturing Fluids as an Alternative to Support Geothermal and Fossil Energy Production

AUTHOR NAMES: H. B. Jung,[a] K. C. Carroll,[b] S. Kabilan,[a] D. J. Heldebrant,[a] D. Hoyt,[a] L. Zhong,[a] T. Varga,[a] S. Stephens,[a] L. Adams,[a] A. Bonneville,[a] A. Kuprat[a] and C. A. Fernandez[a]*

AUTHOR ADDRESSES:

[a] Pacific Northwest National Laboratory, Richland, WA 99352.
[b] New Mexico State University, Las Cruces, NM 88003.

*carlos.fernandez@pnnl.gov

Figures: S1-S17

Tables: S1

Table S1. Polymers examined for rheology and volume expansion (1 wt% aqueous solutions) including experimental conditions of temperature and pressure.

Polymer	Chemical Formula	Temperature °C	Pressure atm	Gel Formation	Volume Change %[1]
3-[(2-aminoethyl) amino] propylmethoxysiloxane dimethylsiloxane copolymer with 2–4% amino content	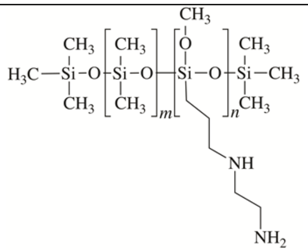	365–371	140–300	No	Neligible
3-aminopropylmethylsiloxane-dimethylsiloxane copolymer with 6–7% amino content	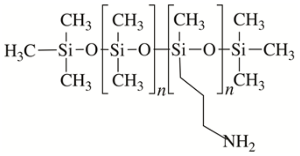	358–372	160–300	No	Neligible
3-aminopropyl-terminated polydimethylsiloxane with 3.2–3.8% amino content	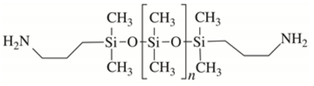	368–369	155–300	No	Neligible
Poly(allylamine) solution average MW ~17,000 20 wt% in H_2O	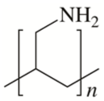	353–369	130-300	Yes	(150 ± 10) %

1. Based on three replicas

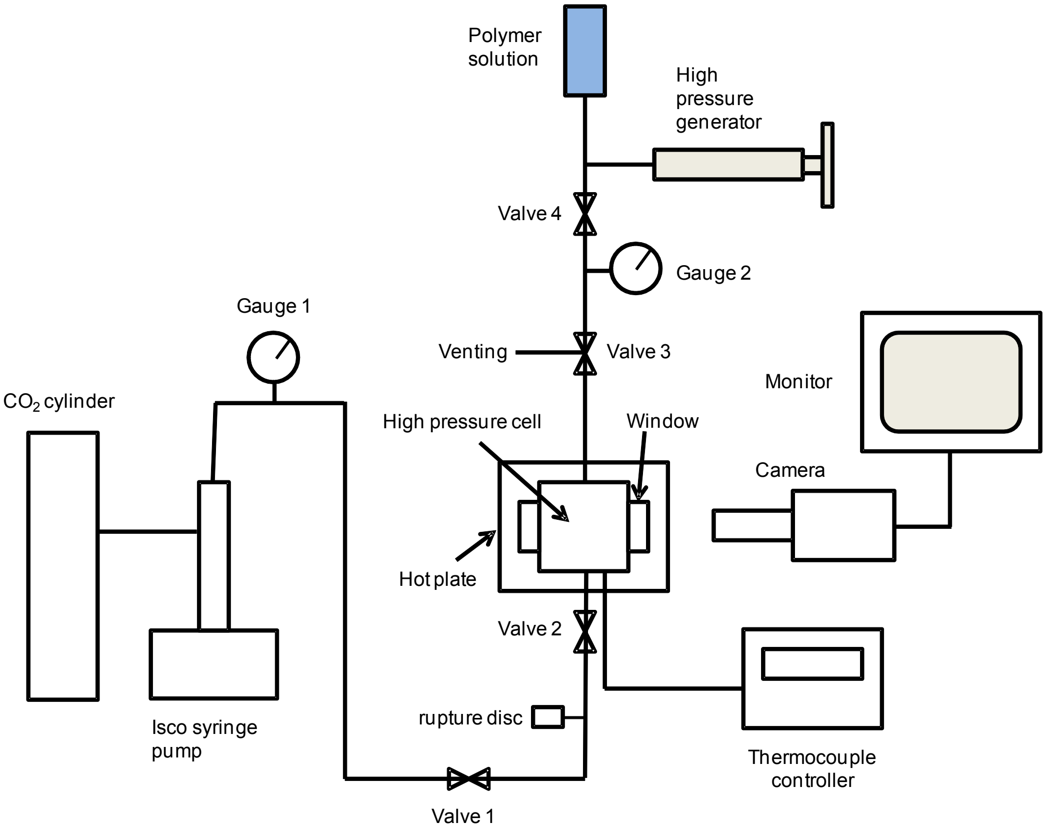

Fig. S1. Schematic diagram of high P-T experimental setup.

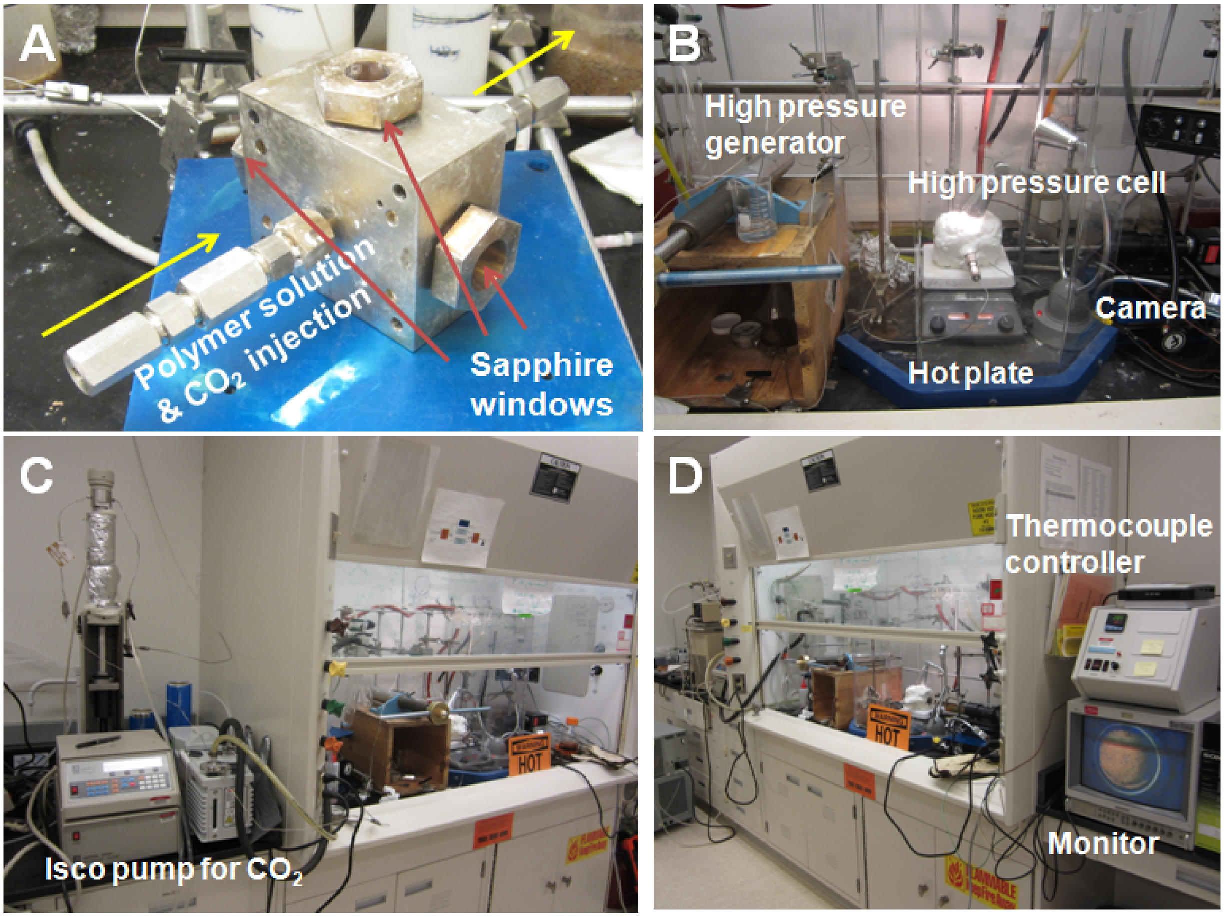

Fig. S2. A: Photo of a high pressure cell with 3 sapphire windows, B-D: Photos of the high P-T experimental setup

High pressure cell temperature calibration

Temperature of the high pressure cell was monitored using a thermocouple (Watlow Electric Manufacturing Company; max. temperature: 1700 °C, accuracy: ±2 °C) attached to the external surface of the high pressure cell. Because of the difference between the internal temperature and the external temperature, an experiment was conducted to estimate the internal temperature based on the external temperature. A thermocouple (Omega Engineering; max. temperature: 750 °C, accuracy: ±2 °C) was inserted into the high pressure cell through the venting hole (Fig. S1), and the internal temperature was compared with the external temperature measured from the surface of the high pressure cell. The external temperature was increased up to 300 °C, and then deionized water was injected into the cell to completely submerge the thermocouple inserted inside the cell in water. The pressure was 155 atm at the external temperature of 300 °C without addition of CO_2. In this experiment, the cell was not pressurized with CO_2 for the sake of safety. After the heat was turned off, both external and internal temperatures were monitored simultaneously while the temperatures decreased. The internal and external temperatures were monitored as the external temperature decreased from 300 ºC to 60 °C, which corresponded to the internal temperature decrease from 402 ºC to 73 ºC (Fig. 2). At the external temperature interval between 60 °C and 300 °C, there was a strong linear correlation between external temperature and internal temperature ($R^2 = 0.999$; $n = 18$), which showed higher internal temperature than external temperature. Therefore, internal temperatures in the following experiments were estimated based on the linear relationship and external temperatures measured using a thermocouple.

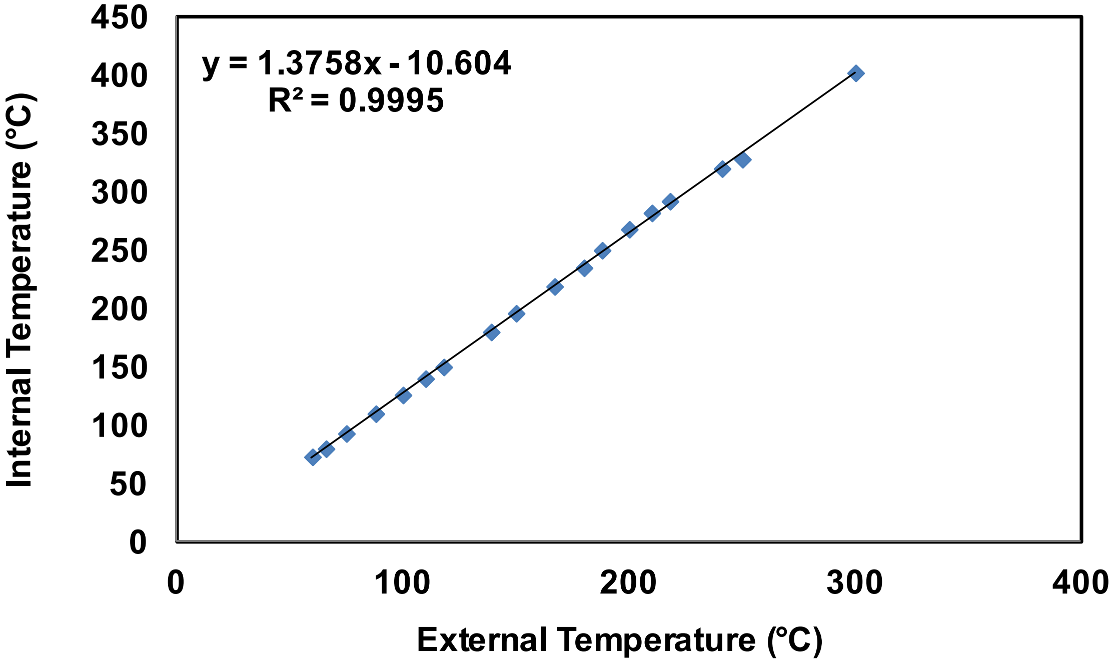

Fig. S3. Relationship between external temperature and internal temperature for the high pressure cell

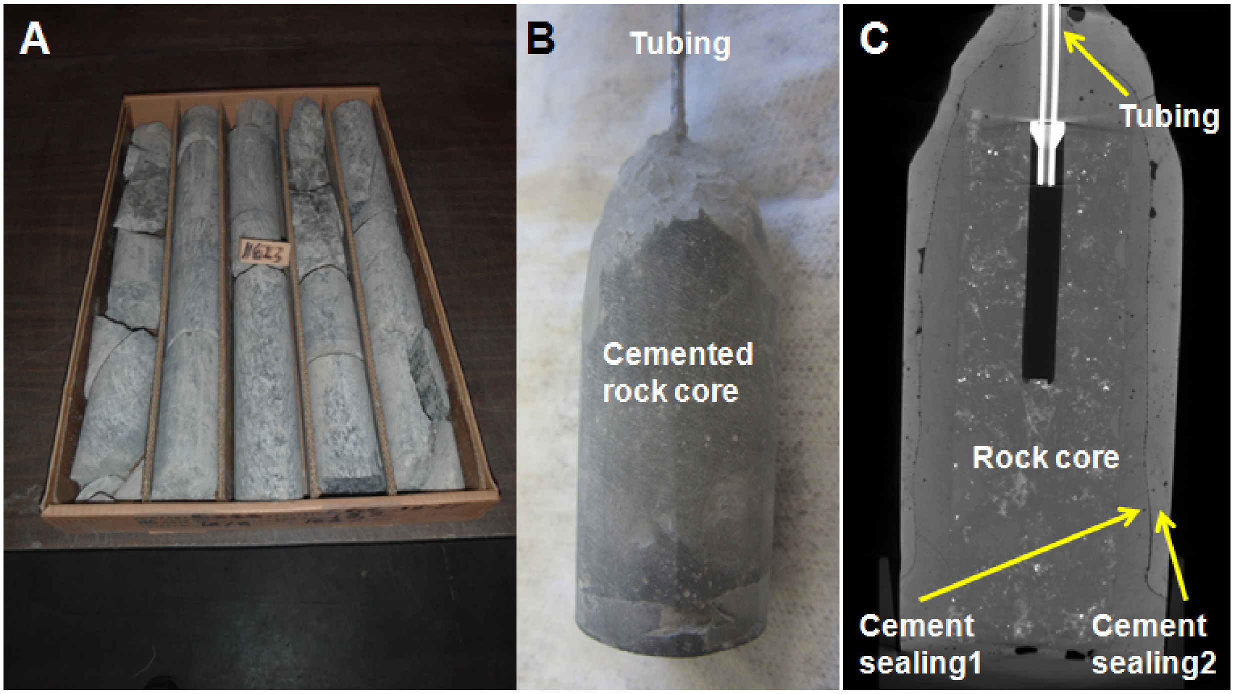

Fig. S4. A: Picture of raw rock cores collected from Coso geothermal field. B: Picture of a cemented rock core (0.625” D and 2” L) with HIP tubing (1/16” OD) for hydraulic fracturing experiment. B: XMT image of a cemented rock core; A few days after cementing the rock core, additional cement layer covered the rock core to maximize the sealing under high confining pressure (204 atm).

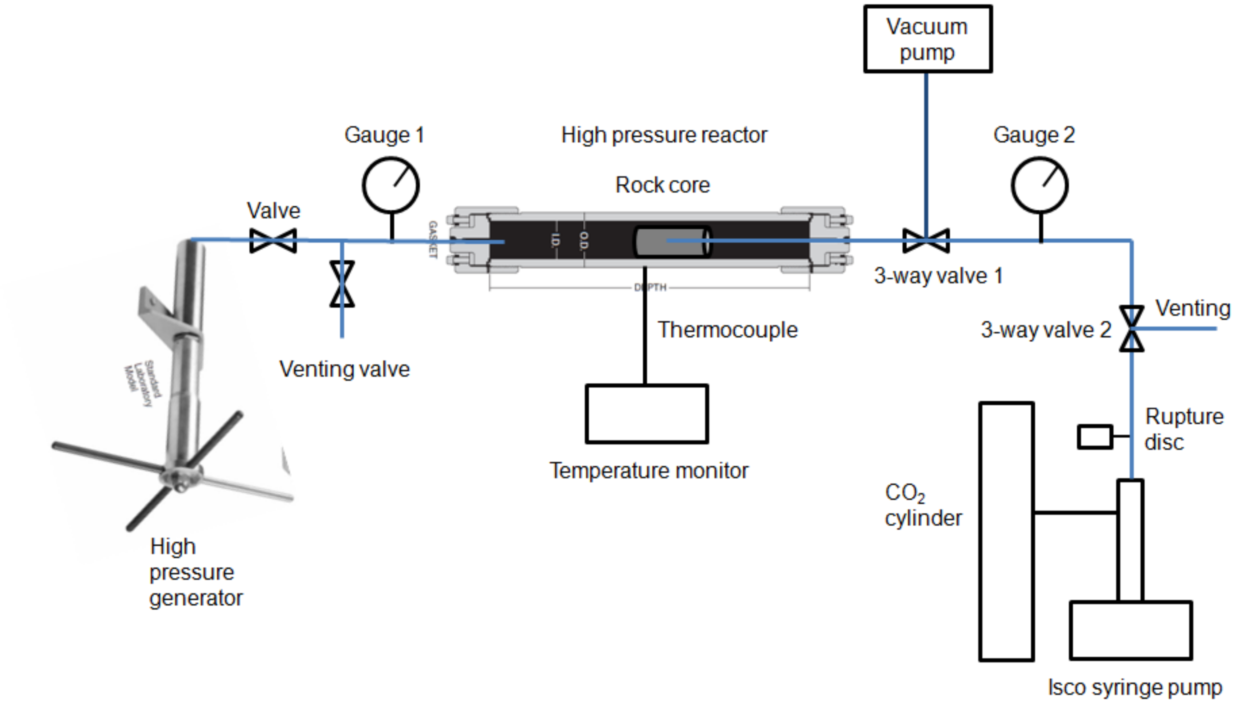

Fig. S5. Schematic diagram for the hydraulic fracturing experimental setup.

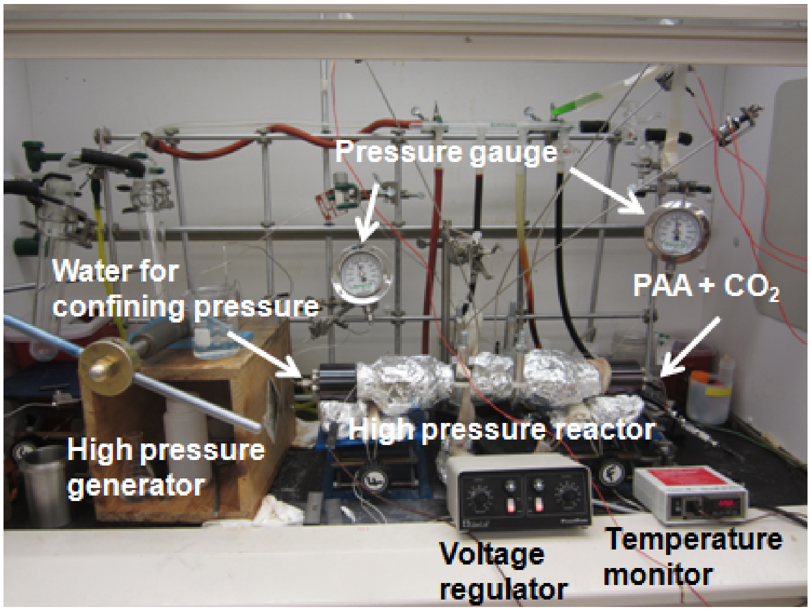

Fig. S6. Photo showing the experimental setup for hydraulic fracturing.

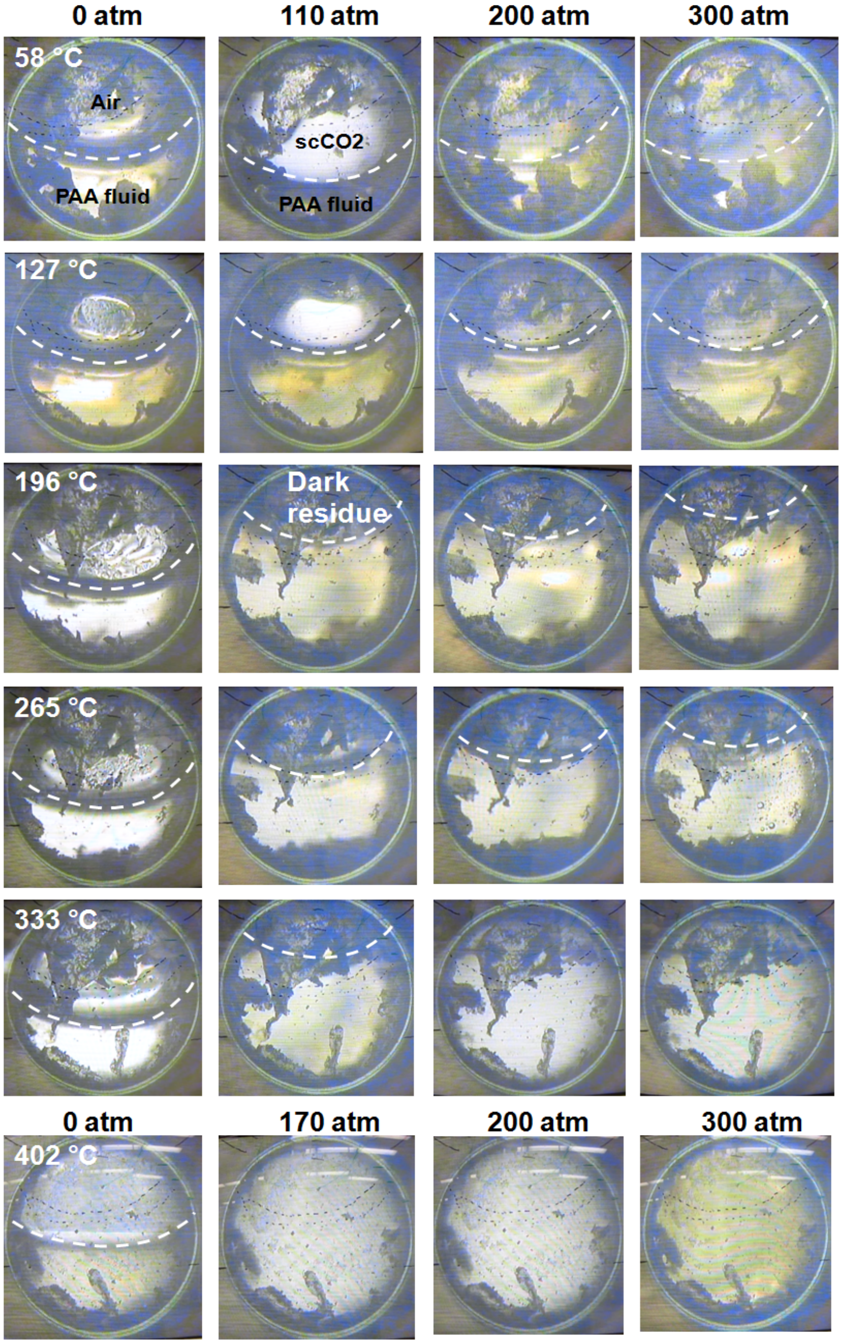

Fig. S7. Volume changes of PAA solution reacted with CO_2 as a function of temperature (58–402°C) and CO_2 pressure (0–300 atm). CO_2 pressure was increased from 110 to 300 atm, except for the experiment at 402°C (170–300 atm), where the initial pressure of PAA solution at 402°C was 150 atm before CO_2 injection. The dashed lines indicate the boundary between PAA fluid and supercritical CO_2 (after CO_2 injection) or air/water vapor (before CO_2 injection). The window is partially covered by some residual PAA. Compare these results with Figure S8 for DIW/CO_2.

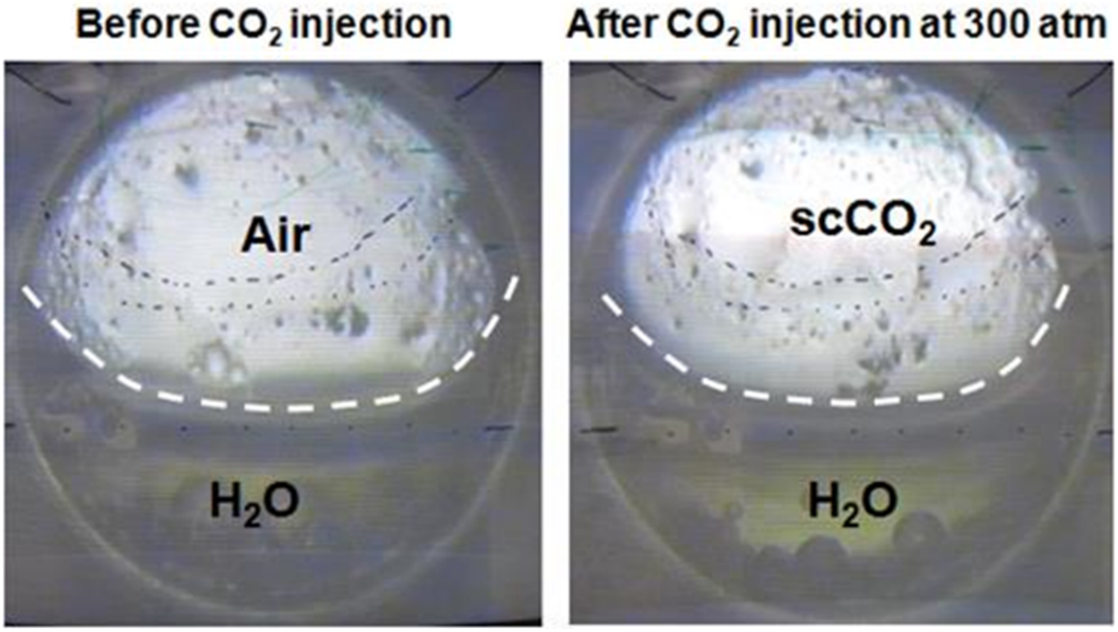

Fig. S8. The volume and rheology changes of deionized water after CO_2 injection at 333 ºC. The bottom half is deionized water and the top half is air or supercritical CO_2.

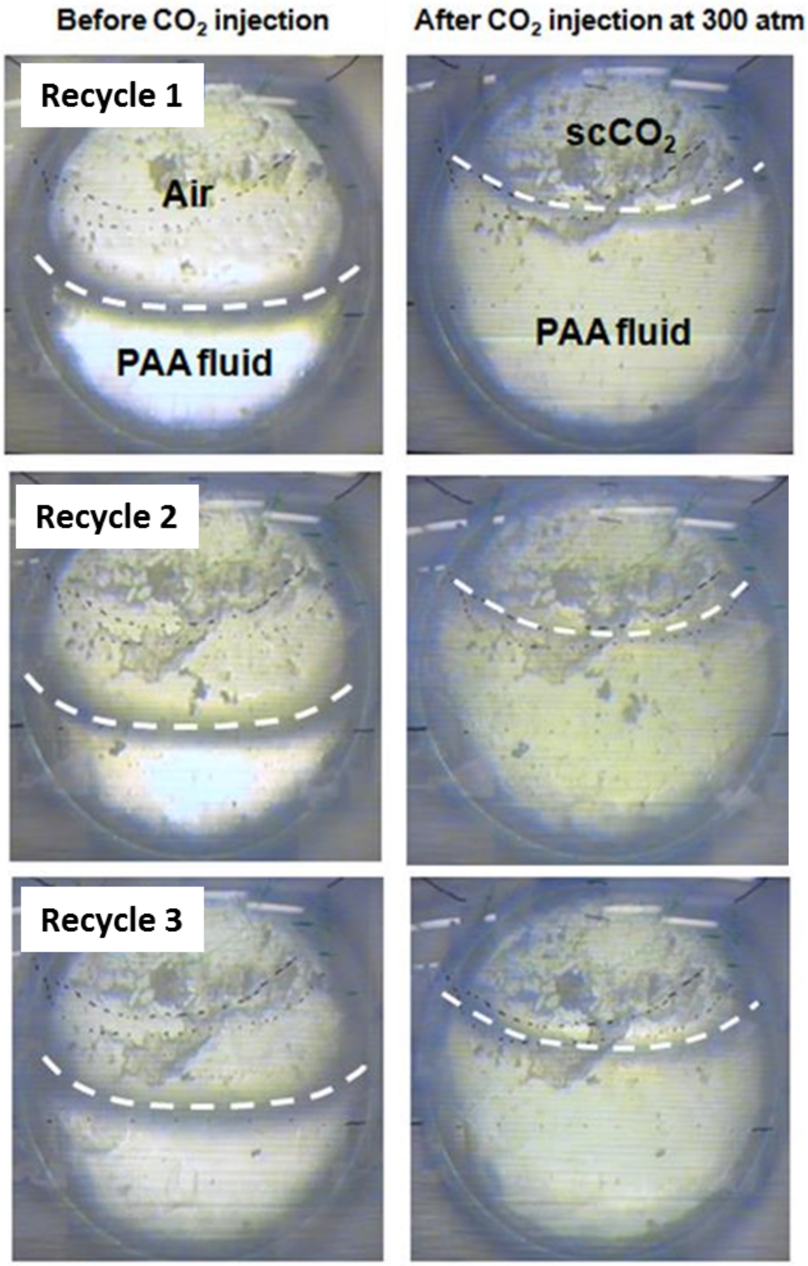

Fig. S9. Volume changes of recycled PAA solution (1 wt%) before and after CO_2 injection. Some PAA was not dissolved back and may be the reason for the observed smaller volume expansion observed on the third recycle as compared to the first recycle.

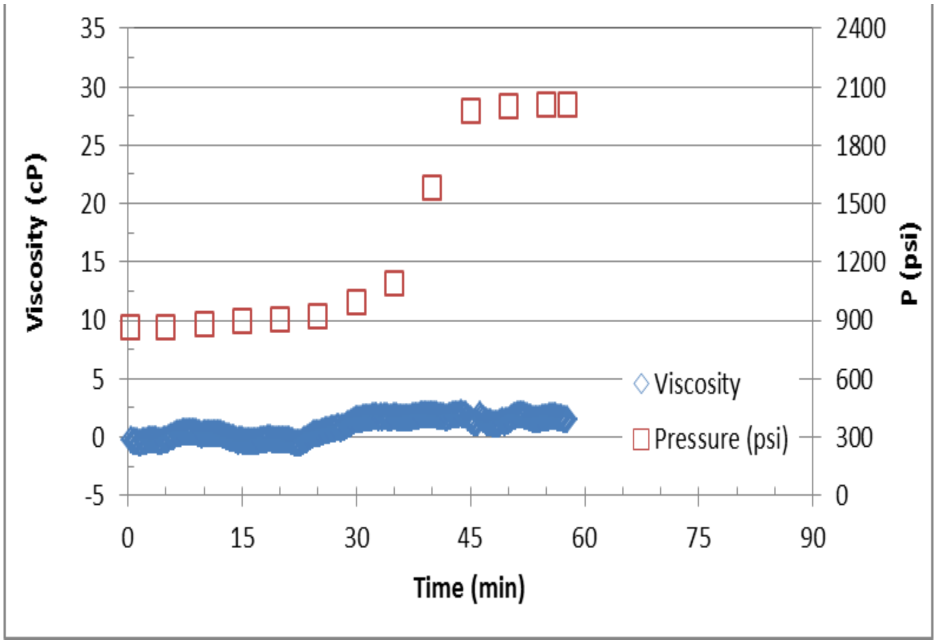

Fig. S10. Viscosity of deionized water-CO_2 mixture as a function of CO2 pressure at 190 ºC (shear rate 100 s^{-1})

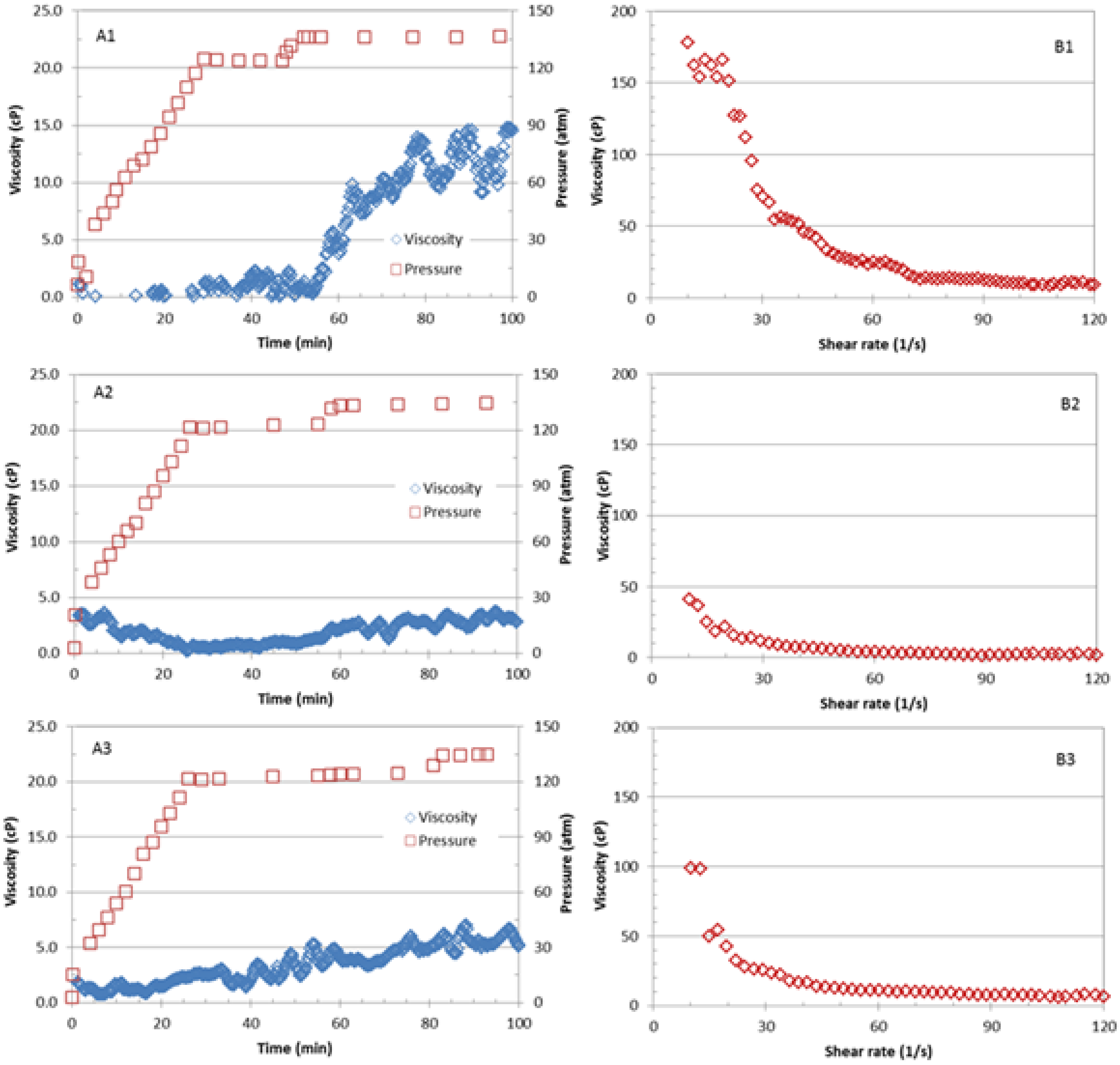

Fig. S11 Comparison of fluid viscosity as a function of CO_2 pressure at 190°C and 100 s^{-1} shear rate (left) and as a function of shear rate at 190°C and 130 atm (right). A1 and B1: 1% PAA solution; A2 and B2: 0.1% xanthan gum solution; A3 and B3: 1% SDS solution. It is important to note that the instrument P/T limits are far below the pressure and temperatures required for the aqueous PAA- CO_2 fluid to transition to a hydrogel.

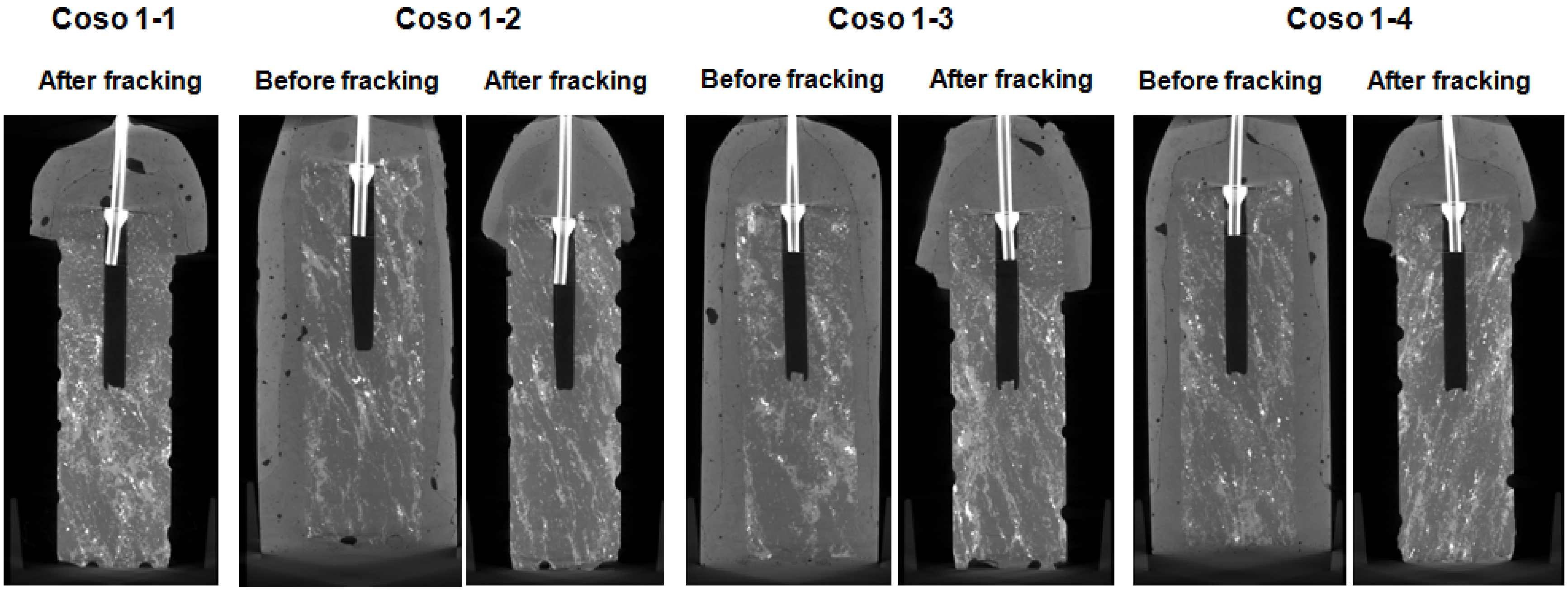

Fig. S12. XMT images of rock cores from Coso geothermal site, CA before and after hydraulic fracturing experiment using 1 wt.% PAA and CO2 (Coso 1-1 and 1-2), 1 wt.% SDS and CO2 (Coso 1-3), and distilled water and CO2 (Coso 1-4). No XMT image is available for Coso 1-1 before hydraulic fracturing experiment.

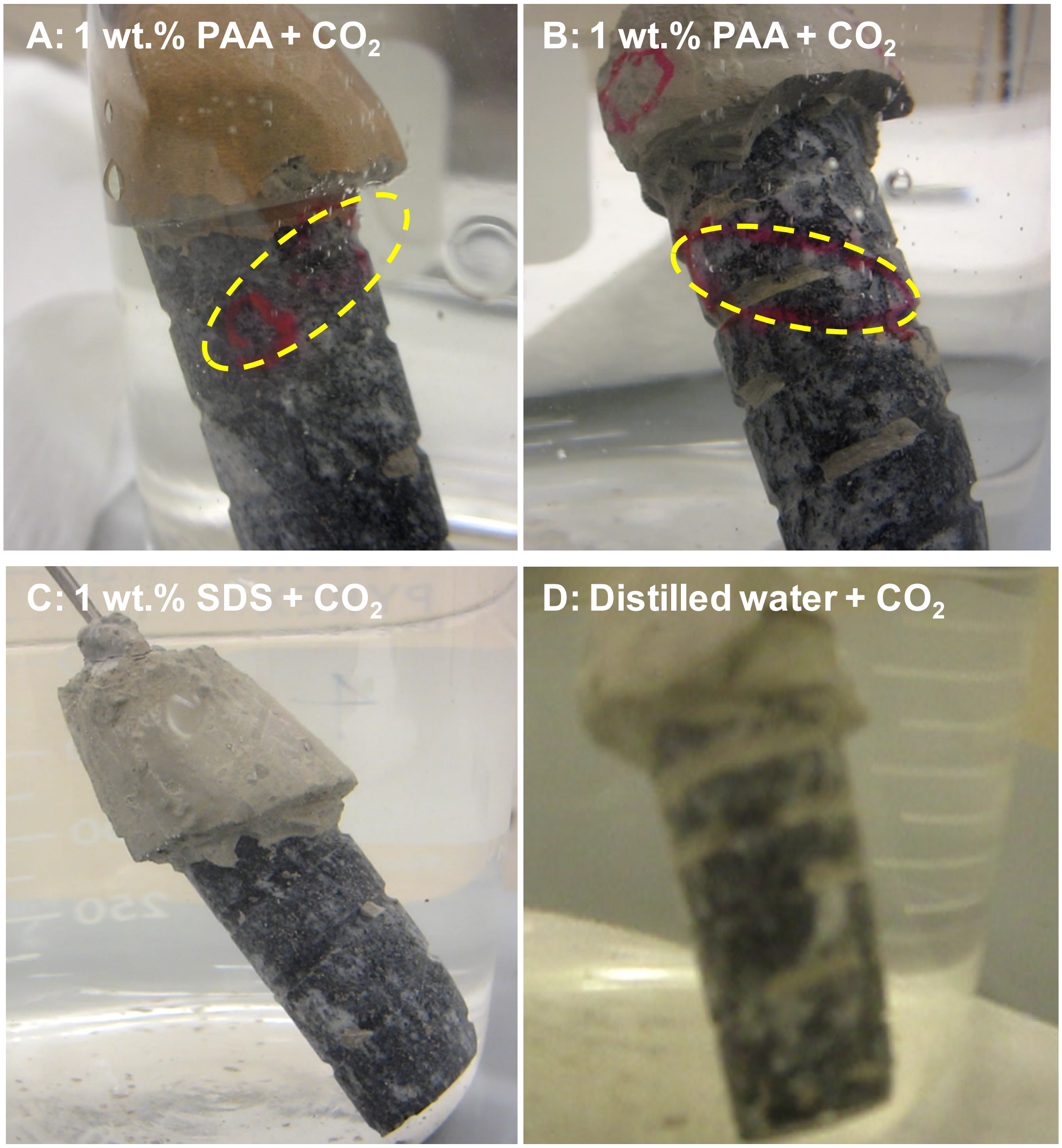

Fig. S13. Pictures of CO_2 leakage experiment at ~5 atm CO_2 pressure. CO_2 bubbling from the rock surface was observed from the rock cores Coso 1-1 and Coso 1-2 (photos A and B) after hydraulic fracturing experiment with 1 wt.% PAA and CO_2. No evidence of fractures was observed for DIW and CO_2 or 1 wt% aqueous SDS and CO_2 (photos C and D).

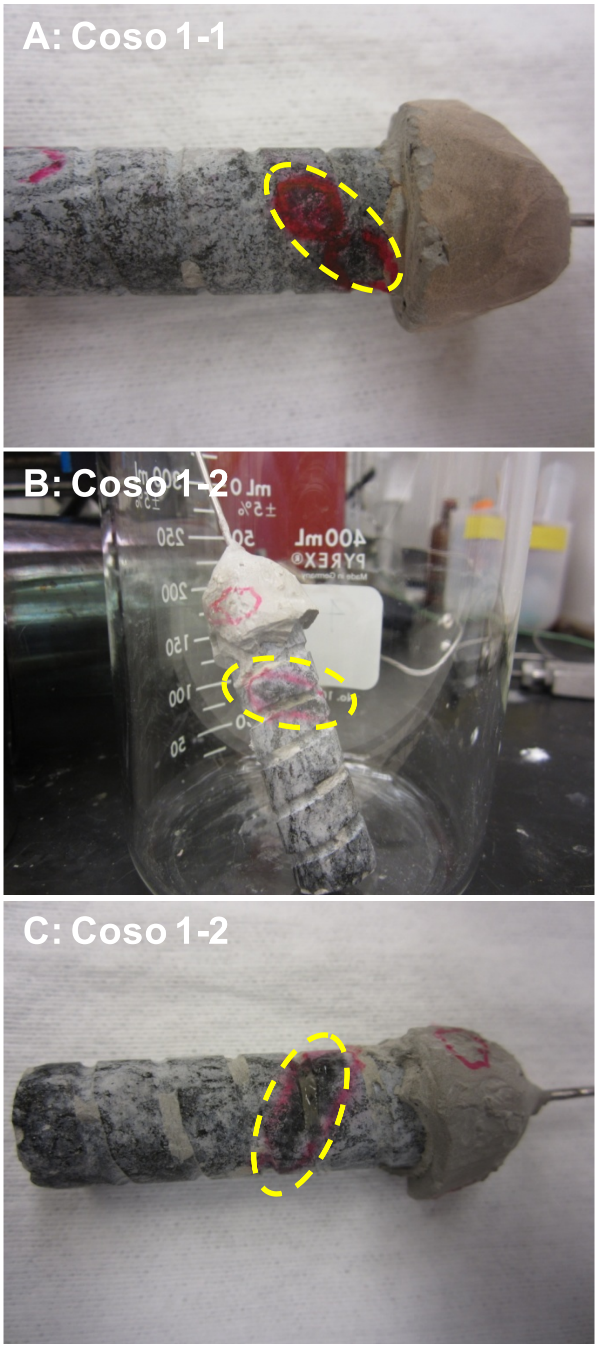

Fig. S14. Pictures of the injection of KI solution (0.3 g/mL) into the rock cores at ~7 atm N_2 after the hydraulic fracturing experiment with 1 wt.% PAA and CO_2. The seepage of KI solution occurred through the fractured rock surface.

Fig. S15. Time-series of the seepage of the KI solution injected into the rock core (Coso 1-2) at ~7 atm N_2 pressure. The seepage of KI solution occurred on the upper left side of the rock surface within the red mark in 15 seconds, and then the seepage of KI solution occurred along a line within the red mark, which is presumed to be micro-fractures.

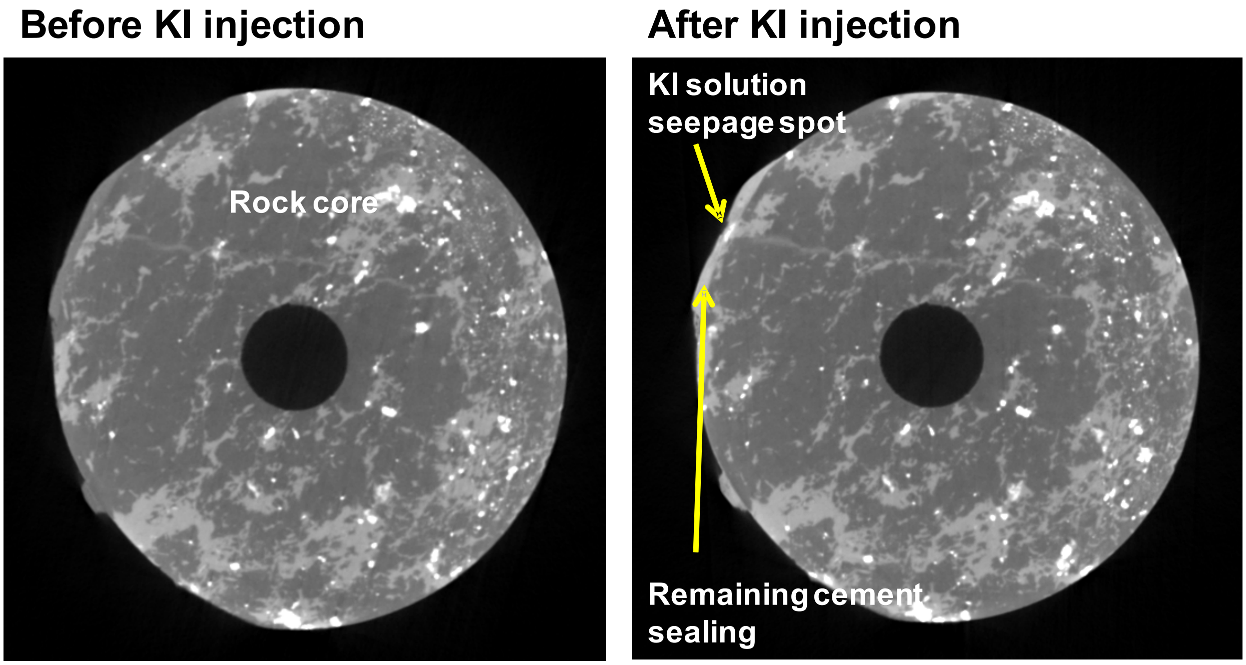

Fig. S16. XMT images of a horizontal slice of the fractured rock core (Coso 1-2) before and after the injection of KI solution (0.3 g/mL) at 7 atm N_2 pressure. After the injection of KI solution, the cement sealing remaining on the outside surface of the rock core became brighter because of the seepage of KI solution.

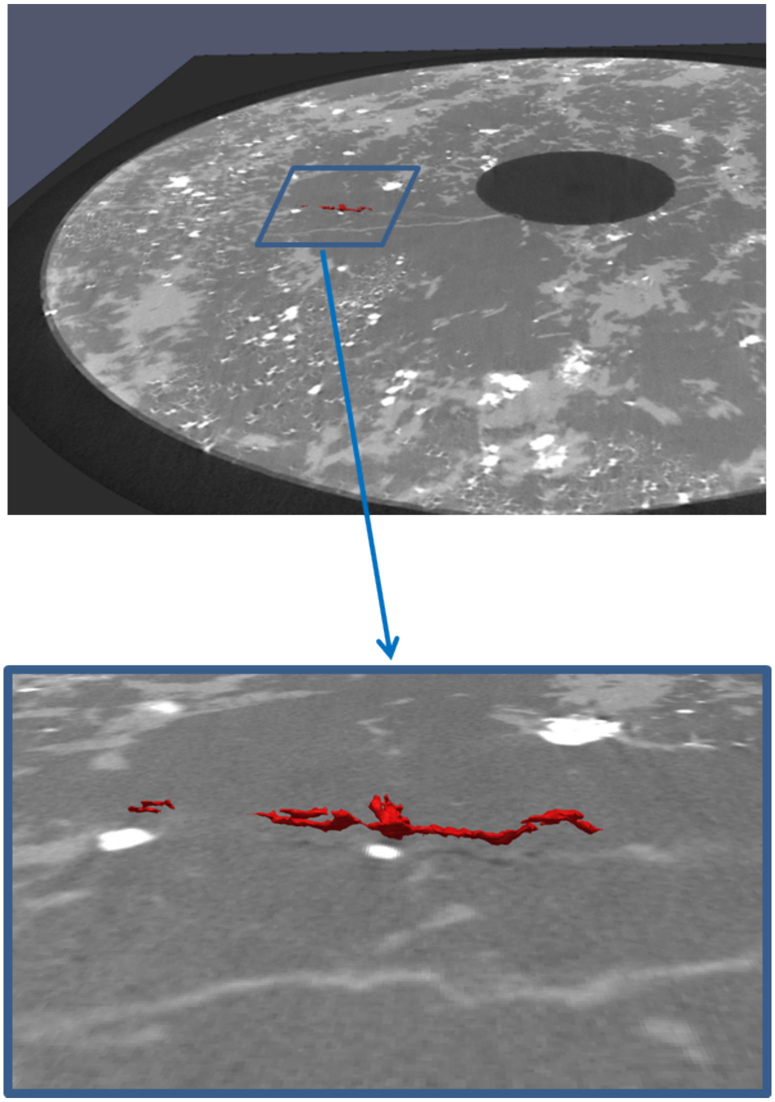

Fig. S17. XMT image of a volume spanning 20 horizontal XMT slices on the fractured rock core (Coso 1-2) showing the presence of a local fracture created at 4 atm differential pressure. It is important to note, that although the fracture seems not to connect the internal void volume of the rock with its external surface, microfractures smaller than the resolution limit of the instrument are present and allow fluid flow through the rock as evidenced by CO_2 and KI flow experiments.